Supporting Information for "Is the Madden-Julian Oscillation a Moisture Mode?"

Víctor C. Mayta[1] *, Ángel F. Adames Corraliza[1]

[1]Department of Atmospheric and Oceanic Sciences, University of Wisconsin, Madison, Wisconsin

Contents of this file

1. Text S1 to S4
2. Table S1
3. Figures S1 to S3

*Department of Atmospheric and Oceanic Sciences, University of Wisconsin, 1225 W Dayton St, Madison, WI 53706, USA.

a. Wave-type filtering of CLAUS T_b

To isolate individual components of the MJO, T_b is filtered following the method proposed by Wheeler and Kiladis (1999) using the same frequency-wavenumber boxes documented in previous works (Kiladis et al., 2009). This is accomplished in the wave number-frequency domain by retaining only those spectral coefficients within a specific range corresponding to the spectral peaks associated with a given mode. The filter settings for the 20-96-days period and wavenumbers $k = 0 - 2$, $k = 3 - 10$, and $k = 0 - 10$.

b. Phase speed calculation: A Radon Transform Approach

The Radon Transform was been used in recent years as more objective way to calculate the phase of the waves (e.g., Yang et al., 2007; Mayta et al., 2021; Mayta & Adames, 2021; Mayta et al., 2022). The Radon Transform of $g(x, y)$ is the integral of g along the line L oriented at angle θ, with angles ranging from 0° to 180°. A detailed schematic and explanation of each variable can be found in Fig. A1 of Mayta et al. (2021). Thus, the Radon Transform can be defined as a projection of $g(x, y)$ on L as follows:

$$P(s, \theta) = \int_u g(x, y) du \tag{S1}$$

where u is the direction orthogonal to L, and s is the coordinate on L. Thus, for a given angle θ, the Radon Transform is a function of the line coordinate s. From these considerations and rewriting equation S1 above in terms of coordinates x and y,

$$p(x', \theta) = \int_{y'} f(x, y) \Big| \begin{Bmatrix} x = x' cos\theta - y' sin\theta \\ x = x' sin\theta - y' cos\theta \end{Bmatrix} dy' \tag{S2}$$

the phase speed is expressed by finding the value of θ or θ_{max}, for which $\int p^2 f(s,\theta)ds$, when p from equation S2 is a maximum. Finally, the phase speed c_p is then calculated as follows,

$$c_p = \frac{tan(\theta_{max}) \times \Delta x \times 111.319km \times cos(\varphi)}{\Delta t} \tag{S3}$$

where 111.319 km $\times$ $cos(\varphi)$ is the length of a degree longitude at latitude φ. The phase speed c_p is obtained based on the temporal (Δt) and spatial (Δx) resolution of the data considered in the time-longitude calculation. Table S1 summarizes the phase speed calculated for different regions.

c. Calculation of cloud-radiation feedback parameter (r) and Effective Gross Moist Stability (m_{eff})

In this study, we calculated m_{eff} from a scatterplot of anomalous $\langle \omega \partial_p m \rangle$ and $\langle Q_r \rangle$ against $\langle \omega \partial_p s \rangle$ as in Inoue and Back (2017):

$$m_{eff} = \underbrace{\frac{\langle \omega \partial_p m \rangle}{\langle \omega \partial_p s \rangle}}_{\Gamma} - \underbrace{\frac{\langle Q_r \rangle}{\langle \omega \partial_p s \rangle}}_{r} \tag{S4}$$

Figure S2 shows scatterplots for the calculation of m_{eff} for two distinct regions: Indo-Pacific warm pool (60°E–180°) and Eastern Pacific-Atlantic (120°W–0°). Γ shows relatively different values in both regions with a higher value over Eastern Pacific- Atlantic ($\Gamma \approx 0.35$) than Indo-Pacific ($\Gamma \approx 0.18$). The cloud-radiation feedback parameter is depicting close values in both regions, with $r = 0.13$ and $r = 0.07$ for the warm pool and Eastern Pacific - Atlantic region, respectively. Thus, from Eq. (S4) and Figures S2c, f, is possible to infer that the m_{eff} results in different values associated with the MJO over

both regions. We obtain a value of $m_{eff} = 0.05$ for the warm pool region (Fig. S2c) and $m_{eff} = 0.28$ for the Eastern Pacific - Atlantic region (Fig. S2f).

d. The Moisture Mode Cutoff Wavenumber (k_{moist}) definition

To determine the cutoff wavenumber (k_{moist}) in which the transition occurs between convective quasi-equilibrium (QE) and WTG, we use the relation proposed in recent work (see Eq. 51 in Ahmed et al., 2021),

$$k_{moist} \approx 2\frac{\sqrt{m_{eff}\varepsilon_a\varepsilon_q}}{c} \tag{S5}$$

where m_{eff} is the effective gross moist stability, $\varepsilon_q = 1/\tau_c$ is the convective moisture sensitivity, and

$$\varepsilon_a = \varepsilon_q + \varepsilon_t(1 + r) \tag{S6}$$

is the inverse of the effective convective adjustment time scale. In Eq. (S6) ε_t is temperature sensitive and r cloud-radiative feedback parameter. In the section above, we found values of r close to zero for the MJO (Figures S2c, f), which is also in agreement with previous studies (e.g., Inoue et al., 2020). By considering this approximation, Eq. (S6) takes the form of

$$\underbrace{\varepsilon_a}_{\tau_a^{-1}} \approx \underbrace{\varepsilon_q}_{\tau_q^{-1}} + \underbrace{\varepsilon_t}_{\tau_t^{-1}} \tag{S7}$$

with these definitions, Eq. (S5) takes the following form

$$k_{moist} \approx \frac{2}{c}\sqrt{\frac{m_{eff}(\tau_t + \tau_q)}{\tau_q^2\tau_t}} \tag{S8}$$

Eq. (S8) represents a simplified version of the calculation of the moisture mode cutoff wavenumber (k_{moist}) after scale analysis associated with the MJO.

References

Adames, Á. F. (2022). The Basic Equations Under Weak Temperature Gradient Balance: Formulation, Scaling, and Types of Convectively-coupled Motions. *Journal of the Atmospheric Sciences*, *79*(8), 2087 - 2108. doi: 10.1175/JAS-D-21-0215.1

Ahmed, F., Neelin, J. D., & Adames, Á. F. (2021). Quasi-equilibrium and weak temperature gradient balances in an equatorial beta-plane model. *Journal of the Atmospheric Sciences*, *78*(1), 209 - 227. doi: 10.1175/JAS-D-20-0184.1

Inoue, K., Adames, Á. F., & Yasunaga, K. (2020). Vertical Velocity Profiles in Convectively Coupled Equatorial Waves and MJO: New Diagnoses of Vertical Velocity Profiles in the Wavenumber-Frequency Domain. *Journal of the Atmospheric Sciences*, *77*(6), 2139 - 2162. doi: 10.1175/JAS-D-19-0209.1

Inoue, K., & Back, L. E. (2017). Gross moist stability analysis: Assessment of satellite-based products in the gms plane. *J. Atmos. Sci.*, *74*(6), 1819-1837. doi: 10.1175/JAS-D-16-0218.1

Kiladis, G. N., Wheeler, M. C., Haertel, P. T., Straub, K. H., & Roundy, P. E. (2009). Convectively coupled equatorial waves. *Reviews of Geophysics*, *47*(2).

Mayta, V. C., & Adames, A. F. (2021). Two-day Westward-Propagating Inertio-Gravity Waves during GoAmazon. *Journal of the Atmospheric Sciences*, *78*(11), 3727–3743. doi: 10.1175/JAS-D-20-0358.1

Mayta, V. C., Adames, Á. F., & Ahmed, F. (2022). Westward-propagating Moisture Mode over the Tropical Western Hemisphere. *Geophysical Research Letters*, e2022GL097799.

Mayta, V. C., Kiladis, G. N., Dias, J., Dias, P. L. S., & Gehne, M. (2021). Convectively Coupled Kelvin Waves Over Tropical South America. *Journal of Climate*, *34*(16), 6531 - 6547. doi: 10.1175/JCLI-D-20-0662.1

Wheeler, M., & Kiladis, G. (1999). Convectively-coupled equatorial waves: Analysis of clouds in the wavenumber-frequency domain. *J. Atmos. Sci.*, *56*, 374–399.

Yang, G.-Y., Hoskins, B., & Slingo, J. (2007). Convectively coupled equatorial waves. Part II: Propagation characteristics. *J. Atmos. Sci.*, *64*, 3424–3437.

Table S1. Phase speeds propagation of the MJO considering different regions of propagation. The θ_{max} values used in the Eq. (S3) are shown for each corresponding longitude.

Region	Convection (Lon)	θ_{max}	Phase speed (m s^{-1})
Western Pacific	180° to 140°W	58.8 °	5.95
Eastern Pacific	140°W to 95°W	74.3°	12.80
Atlantic	95°W to 0°	67.0°	8.50
Africa	0° to 55°E	61.3°	6.60
Western Indian Ocean	55°E to 100°E	48.8°	4.12
Eastern Indian Ocean	100°E to 140°E	51.3°	4.50
Maritime Continent	55°E to 100°E	49.6°	4.24

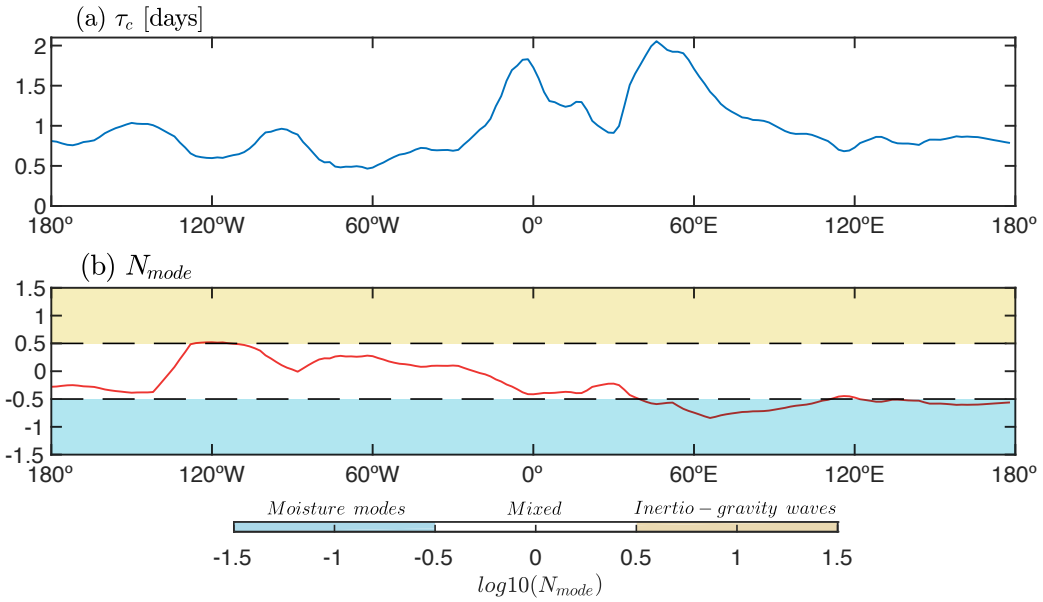

Figure S1. (Top) Geographical variation of the convective moisture adjustment time scale ($\tau_c = \langle q' \rangle / P'$) and the dimensionless N_{mode} parameter (bottom). Shadings in panel (b) represent base 10 logarithm of N_{mode} as in Adames (2022), where blue represents N_{mode} values categorized as moisture modes, yellow can be considered inertio-gravity waves, and white represents mixed systems.

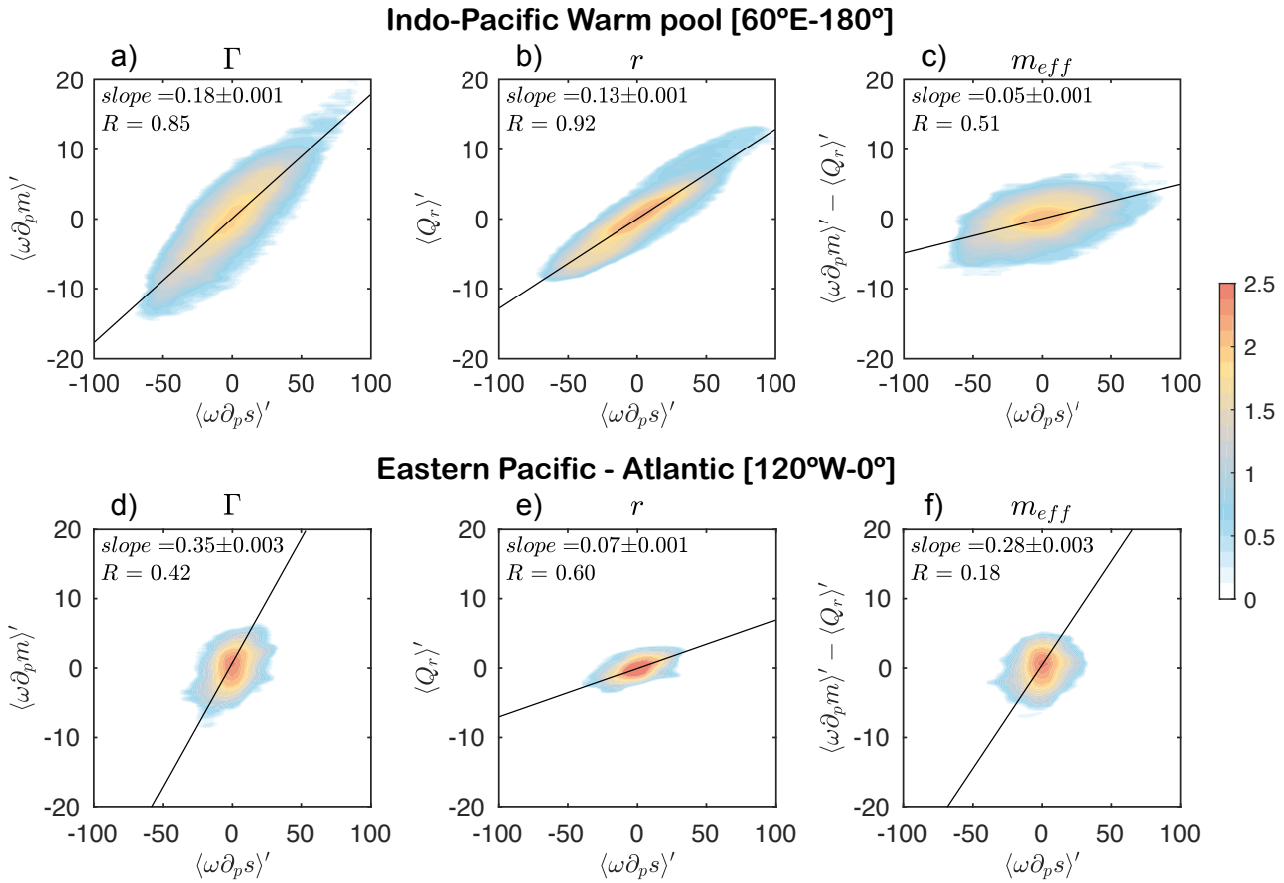

Figure S2. Scatterplot of (a, d) vertical advection of MSE ($\langle\omega\partial_p m\rangle'$), (b, e) column radiative heating ($\langle Q_r\rangle'$), and (c, f) their difference ($\langle\omega\partial_p m\rangle' - \langle Q_r\rangle'$) as a function of column DSE ($\langle\omega\partial_p s\rangle'$). The slope of the linear least squares fitting represents the gross moist stability (Γ), cloud-radiation feedback (r), and the effective GMS (m_{eff}). The shading represents the base-10 logarithm of the number of points within 0.5 W m^{-2} × 5 W m^{-2} bins. Anomalies are computed over the tropical belt domain (10°S–10°N) and for two separated regions: (a)-(c) Indo-Pacific Warm pool (60°E–180°); and (d)-(f) Eastern Pacific - Atlantic . The slope of the linear fit and the correlation coefficient are shown in the top-left of each panel.

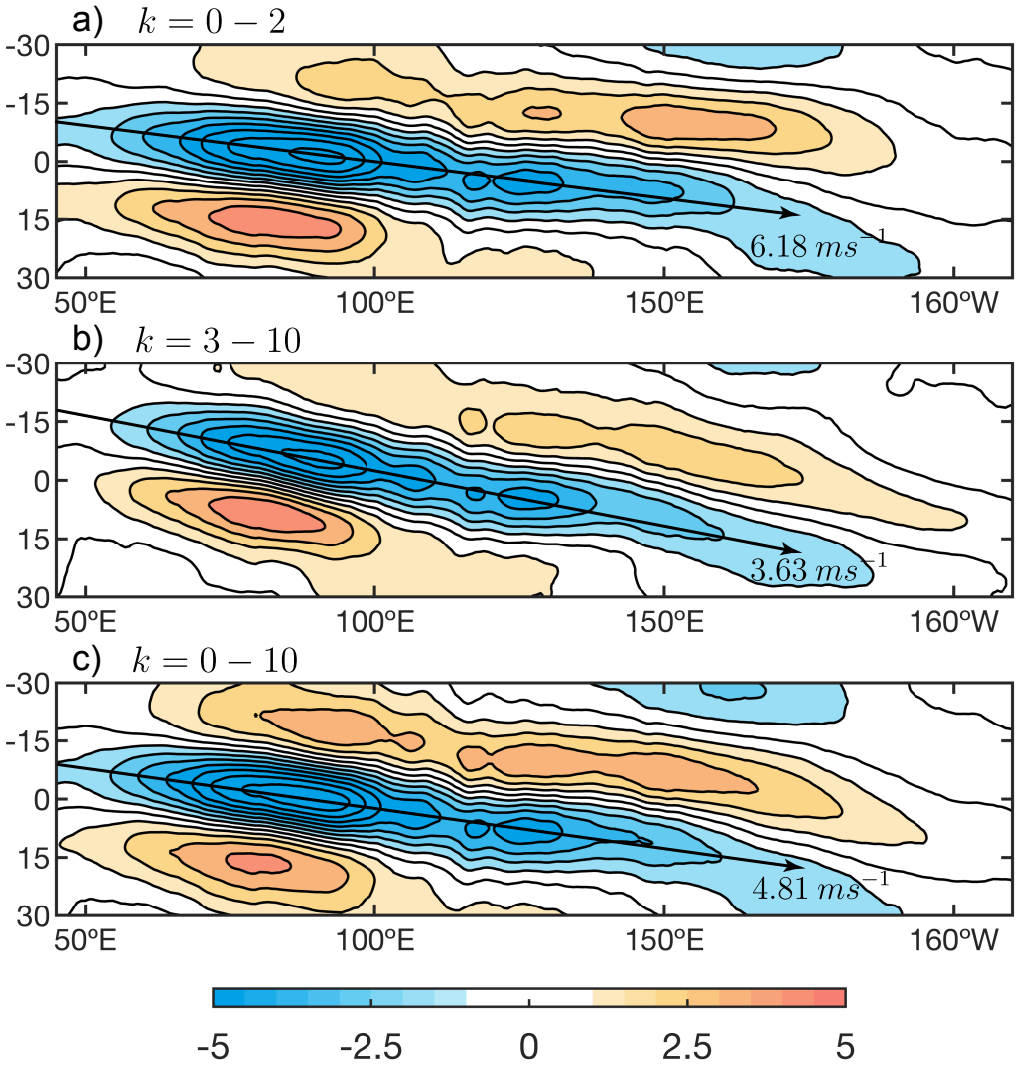

Figure S3. Time-longitude diagram of 10°S–10°N of CLAUS T_b (shading) regressed onto PC1 (normalized) of (a) $k = 0 - 2$, (b) $k = 3 - 10$, and (c) $k = 0 - 10$. The contour interval for T_b is 1 K. The phase speed of the MJO over the Indo-Pacific warm pool region (50°E–160°W) by using the Radon Transform is shown in each plot.